The 2003 Bam, Iran, Earthquake: An Interpretation of the Strong Motion Records

Jafar Shoja-Taheri,[a] Saeid Naserieh,[a] and Amir H. Ghafoorian-Nasab[a]

On 26 December 2003, a destructive earthquake occurred in southeastern Iran, demolishing the city of Bam and vicinity. The highest intensity of shaking (VIII–IX) was observed in the city of Bam. The source of this shock was reported to have had a right-lateral strike-slip mechanism initiated in a blind fault in the north-south direction. A regional network consisting of 23 strong motion stations (SSA-2 Accelerograph), located within 1–290 km from the epicenter, registered the earthquake. The compact and pulse-shape arrivals of strong signals recorded at the Bam station strongly suggest that the rupture was initiated south of the city and propagated toward Bam. Based on the relative arrival times of the rupture front and the arrivals of P and S waves at this station, the velocity of rupture was estimated as 2.5 ± 0.2 km/sec. Comparisons made between the attenuation curves constructed for this earthquake and those of the regional curves show that the effects of directivity caused significant deviations at near distances from the fault. This strong motion data yields estimates of source parameter values of 8.3×0^{25} (dyne -cm), 7.5 km, and 90 bars, respectively, for seismic moment, source radius, and stress drop. [DOI: 10.1193/1.2101887]

INTRODUCTION

On 26 December 2003, a destructive earthquake with an estimated M_w 6.5 occurred in southeastern Iran, demolishing the city of Bam and its neighboring town of Baravat. The death toll was estimated to exceed 40,000. The city of Bam is renowned for the archeological site of *Arg-e-Bam* (Bam Citadel), which comprised the largest sun-dried mud-brick citadel existing in the world and dates back many centuries. This historic site was devastated by the earthquake.

The highest intensity of shaking (VIII–IX) was observed at the city of Bam. This event was the latest in a series of earthquakes on a north-south right-lateral strike-slip system on the west side of the Dasht-e-Lut (Figure 1). This system includes the Gowk fault, which has been the site of five earthquakes since 1981, all of which were associated with co-seismic surface rupture (Adeli 1982; Berberian et al. 1984). There is no documented evidence of historical and instrumentally recorded earthquakes affecting the city of Bam (Ambraseys and Melville 1982).

Talebian et al. (2004) reported that surface displacements mapped using Envistat ra-

[a] Earthquake Research Center, Ferdowsi University of Mashad, Mashad, Iran

Earthquake Spectra, Volume 21, No. S1, pages S181–S206, December 2005;

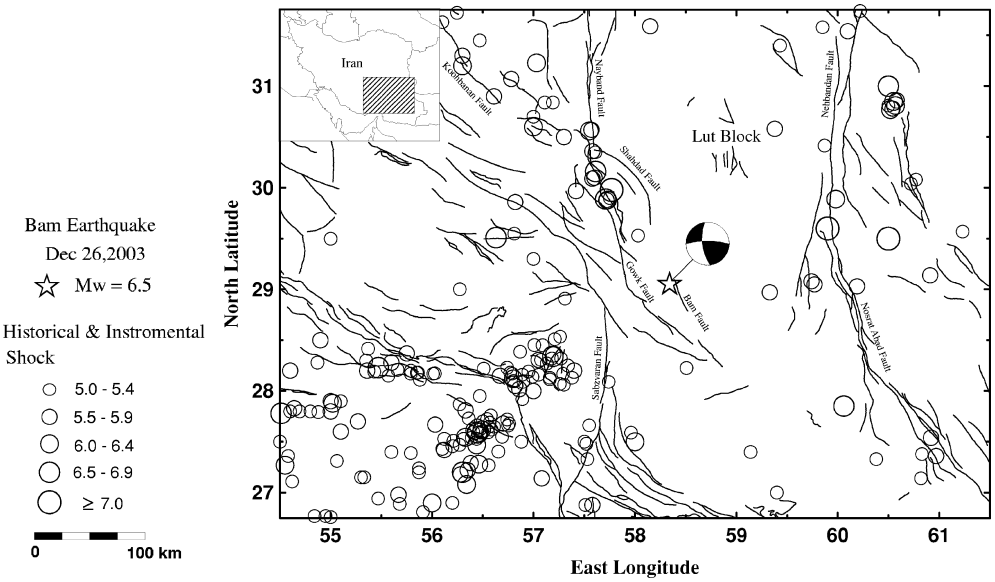

Figure 1. Map of the region adjacent to the Bam, Iran earthquake. Faults were mapped based on the Geological Survey of Iran. Open circles are the locations of historical and instrumental shock prior to the Bam earthquake.

dar data reveal that over 2m of slip occurred at depth on a fault that had not previously been identified, and that there was a complete absence of morphological features associated with the seismogenic of this blind fault that destroyed Bam. To achieve an improved fit to interferogram data obtained in the area, while incorporating teleseismic P- and SH-body wave inversion, a secondary fault was added to the blind fault. It was concluded that this secondary fault was a thrust faulting beneath the previously mapped Bam fault, 5 km to the east of the main rupture. The secondary fault caused a second event approximately 10 seconds after the main shock, with about 20% of the seismic moment of the main strike-slip event. This is consistent with a north-south thrust dipping west at ~30° (Figures 1 and 3b of Talebian et al. 2004). For the strike-slip fault it was found that the most slip occurred over a region that is 12 km long and 8 km wide, with a peak slip of 2.5 m at a depth of ~5 km, decaying to a maximum of 0.5 m in the upper 2 km. The secondary thrust fault slipped up to 1.2 m at depth between the southern end of the main strike-slip fault, and the previously mapped Bam fault.

Nakamura et al. (2004) investigated the hypocenter distribution of aftershocks of the Bam earthquake using a temporal seismic network and found that the hypocenters distribute linearly over ~20 km in parallel with a line 3.5 km west of the previously mapped Bam fault, and extend from the southern area of the city to the heavily damaged eastern part of Bam, including the historic citadel Arg-e-Bam. Based on the distribution of hypocenters, Nakamura et al. proposed a schematic three-dimensional structural model of a new fault, which is in general agreement with the strike-slip blind fault in-

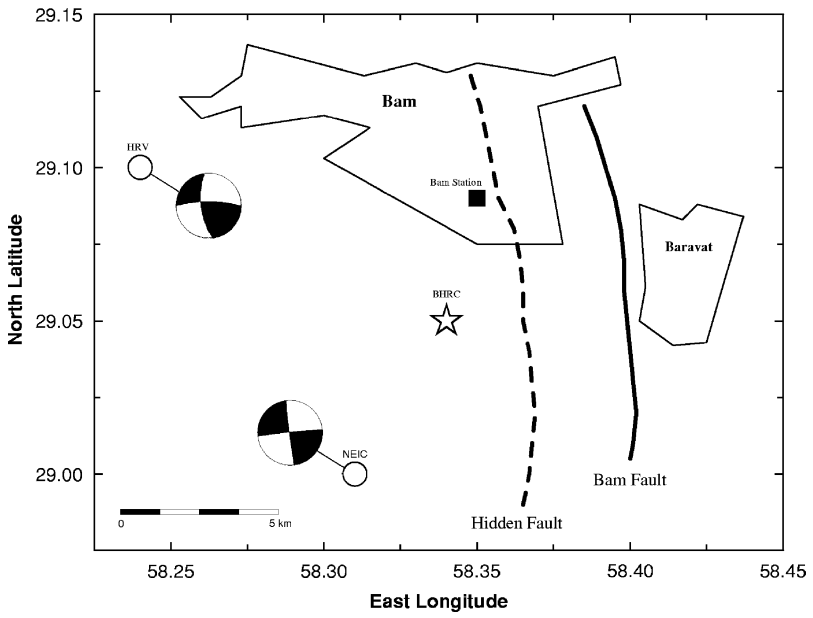

Figure 2. Bam city and the town of Baravat were the areas mostly damaged during the Bam earthquake. The hidden fault shown by the dashed line is inferred by Nakamura et al. (2004). The solid line shows the trace of the previously known Bam fault.

ferred by Talebian et al. (2004). Nakamura et al. suggested that the Bam earthquake occurred not on the Bam fault, but on this new fault (Figure 2). Information regarding the source parameters of this earthquake reported by various investigators is summarized in Table 1.

During this earthquake, a regional network of 74 strong motion accelerograph stations of the Iranian Strong Motion Network (ISMN), maintained by the Building and Housing Research Center (BHRC), was operating (Figure 3). The stations were equipped with SSA-2 instruments. Among these, 23 stations located within a 1–290 km range of the rupture registered the earthquake with peak acceleration of nearly 1.00 to 0.01 g, respectively (Figure 3, Table 2). Soon after the earthquake the staff at ISMN collected and downloaded the recorded strong motion data from the stations and made the uncorrected data available through the BHRC web site (http://www.bhrc.gov.ir) to all interested users.

In the present study, strong motion data were analyzed to illustrate some of the complexities of the source and construct attenuation curves for peak acceleration and velocity. In addition, some of the source parameters were estimated, e.g., stress drops, source dimension, seismic moment, and seismic energy release.

Table 1. Bam earthquake source parameters obtained from previous studies

Date	26 December 2003					
Time	05 hr, 26 min (local time) 01:56:52.4 GMT (NEIS)					
Maximum intensity	VIII to IX (modified Mercalli) (ISMN, 2004)					
	Source Parameters					
Latitude (°N)	Longitude (°E)	Depth (km)	Magnitude	Moment $\times 10^{25}$ dyne−cm	Stress drop bar	Source
29.00	58.31	10	6.5(M_w) 6.8(M_s) 6.0(m_b)	06.6		USGS
29.01	58.24	15	6.6(M_w)	09.3		HARV
			6.6(M_w)	10.0	90	Shoja-Taheri et al. (2004)
29.00	58.29	10	6.5(M_w)	06.8	61	Yagi (2004)
	Focal Mechanism					
Fault plane (Strike, dip, rake)	Auxiliary plane (Strike, dip, rake)					Source
174°, 88°, 178°	264°, 88°, 2°					USGS
172°, 59°, 167°	269°, 79°, 31°					HARV
173°, 63°, 160°	273°, 72°, 29°					Yagi (2004)

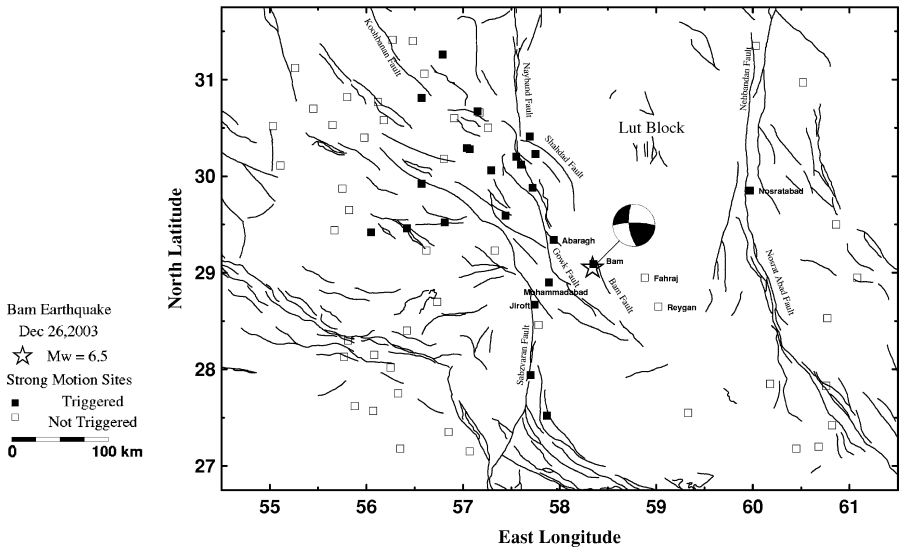

Figure 3. Network of strong motion stations adjacent to the Bam epicentral region.

Table 2. Accelerograph station data from the Bam earthquake

Station	Lat. (°N) Lon.(°E)	Geology[a]	R[b]	R[c]	OR[d]	A_{max} (cm/sec^2)	V_{max} (cm/sec)	M_L	A_0	κ (sec)
Bam	29.10 58.35	Clay alluvium fans	4.5	1.0	278(L)	776.6	122.8	6.3	2.42	0.047
					UP(V)	970.1	39.8		2.10	0.016
					8(T)	623.6	59.4	6.2	2.24	0.041
Mohammad-Abad	28.88 57.90	Alluvium fans	49.1	47.3	350(L)	118.1	11.7	6.8	1.77	0.077
					UP(V)	68.9	2.4		1.20	0.025
					80(T)	70.1	4.0	6.3	1.18	0.026
Abaragh	29.33 57.92	Evaporate and terrace deposits	52.4	46.4	72(L)	158.1	4.6	6.3	0.92	−0.026
					UP(V)	86.6	2.9		0.66	−0.021
					162(T)	102.2	3.8	6.2	0.79	−0.029
Jiroft	28.67 57.73	Terrace deposits	74.1	70.5	240(L)	39.5	4.3	6.5	1.36	0.084
					UP(V)	30.7	1.6		1.15	0.047
					330(T)	27.3	2.9	6.4	1.44	0.092
Rayen	29.59 57.43	Conglomerate and sandstone	107.9	102.2	334(L)	15.0	0.7	6.4	0.70	0.036
					UP(V)	15.2	2.0		0.23	−0.013
					64(T)	13.9	2.8	6.4	0.79	0.036
Golbaf	29.88 57.72	Compacted soil	111.4	103.8	150(L)	30.5	2.1	6.7	1.27	0.069
					UP(V)	13.9	1.2		0.44	−0.001
					240(T)	28.8	2.5	6.5	1.30	0.068
Kahnooj	27.95 57.70	Silt deposits	139.5	133.6	20(L)	11.7	0.6	6.1	0.52	0.025
					UP(V)	8.6	0.3		0.53	0.039
					110(T)	10.1	0.6	6.2	0.65	0.036
Jooshan	30.12 57.58	Compacted soil	140.1	132.3	142(L)	23.5	1.6	6.5	1.44	0.075
					UP(V)	15.3	0.9		0.86	0.031
					232(T)	34.7	2.5	6.6	1.32	0.063
Andoohjerd	30.23 57.75	Compacted soil	144.1	135.9	200(L)	33.7	3.0	6.7	1.35	0.072
					UP(V)	14.9	1.0		0.53	0.008
					290(T)	32.2	1.6	6.6	1.15	0.052

Table 2. (cont.)

Station	Lat. (°N) Lon.(°E)	Geology[a]	R[b]	R[c]	OR[d]	A_{max} (cm/sec^2)	V_{max} (cm/sec)	M_L	A_0	κ (sec)
Sirch	30.19	Compacted soil	150.2	142.4	30(L)	30.6	2.3	6.8	1.26	0.069
	57.56				UP(V)	14.3	0.9		0.75	0.030
					120(T)	29.0	2.1	6.9	1.42	0.091
Mahan	30.06	Cultivated land	153.1	146.0	150(L)	13.0	1.0	6.4	0.95	0.50
	57.28				UP(V)	8.1	0.7		0.61	0.034
					240(T)	13.0	0.9	6.4	0.94	0.054
Lalehzar	29.51	Alluvium fans	159.6	155.6	65(L)	14.3	1.4	6.6	1.05	0.075
	56.82				UP(V)	7.6	0.5		0.43	0.016
					155(T)	13.0	1.2	6.6	1.11	0.082
Shahdad	30.41	Clay and silt	164.7	156.4	78(L)	19.5	2.7	6.9	0.97	0.046
	57.71	deposits			UP(V)	10.1	1.2		0.61	0.027
					168(T)	13.3	1.7	6.8	1.02	0.055
Qalehganj	27.52	Alluvium fans	176.9	170.5	210(L)	22.4	1.3	6.8	1.23	0.063
	57.90				UP(V)	14.3	0.8		0.71	0.030
					300(T)	23.3	1.3	6.7	1.23	0.064
Nosratabad	29.85	Clay and silt	179.1	175.8	284(L)	20.0	2.1	7.1	1.08	0.080
	59.97	deposits			UP(V)	15.4	1.3		0.47	0.032
					14(T)	24.6	2.3	7.2	1.16	0.085
Kerman 2	30.28	Clay deposits	188.2	181.1	140(L)	19.3	2.0	7.0	1.24	0.095
	57.07				UP(V)	8.1	1.1		0.83	0.054
					230(T)	28.4	3.5	7.1	1.23	0.086
Kerman 1	30.28	Clay deposits	188.2	181.1	175(L)	18.2	3.3	7.2	1.06	0.086
	57.07				UP(V)	10.0	0.8		0.61	0.052
					265(T)	24.4	2.8	7.1	0.98	0.082
Cheshmehsabz	29.47	Young alluvium	194.1	190.6	65(L)	23.0	1.1	6.7	1.43	0.104
	56.42				UP(V)	8.1	0.5		0.56	0.039
					155(T)	11.5	1.1	6.6	1.28	0.095

Table 2. (cont.)

Station	Lat. (°N) Lon.(°E)	Geology[a]	R[b]	R[c]	OR[d]	A_{max} (cm/sec^2)	V_{max} (cm/sec)	M_L	A_0	κ (sec)
Bardsir	29.92	Young alluvium	202.7	193.6	75(L)	13.2	1.8	6.9	1.26	0.107
	56.56				UP(V)	5.6	1.1		0.40	0.030
					165(T)	9.7	2.1	6.9	1.02	0.096
Horjand	30.67	Alluvium upper	214.9	207.1	110(L)	6.6	1.3	6.9	0.75	0.084
	57.15	conglomerate and			UP(V)	5.7	1.0		0.46	0.060
		sandstone			200(T)	11.8	1.5	7.0	0.98	0.101
Bolvard	29.42	Decide and	228.4	225.5	145(L)	9.5	0.7	6.6	0.94	0.093
	56.04	quartzite			UP(V)	3.4	0.4		0.42	0.051
					235(T)	9.9	1.0	6.7	1.01	0.100
Zarand	30.81	Silt and clay	259.6	254.0	34(L)	12.0	2.7	7.4	0.55	0.088
	56.57	deposits			UP(V)	5.7	1.0		0.35	0.069
					124(T)	12.9	2.7	7.4	0.71	0.099
Ravar	31.26	Silt and clay	288.7	280.8	320(L)	12.5	1.6	7.3	0.93	0.107
	56.79	deposits			UP(V)	6.7	0.7		0.53	0.030
					50(T)	12.9	1.3	7.4	1.02	0.096

[a] All stations are sited on sedimentary deposit. This column gives the mapped geological unit at the site given by Mirzaei and Farzanegan (1998).
[b] Distance is the epicentral distance for all stations. The epicenter was inferred by the strong motion data.
[c] This column gives the neatest distance to the fault.
[d] Component orientations.

STRONG MOTION DATA

Table 2 lists all the regional strong motion stations that recorded the earthquake. Locations of stations, component orientations, and site geology conditions are taken from Mirzaei and Farzanegan (1998).

Strong motion data of all the stations were processed following the method used by Shoja-Taheri and Anderson (1988). Integration of accelerograms and high-pass filtering of the velocities and displacements were performed in the frequency domain. The filter has the response of that of a Butterworth filter of four poles and corner frequency of 0.125 Hz, but introduced no phase change. The uncorrected data were digitized at the rate of 200 samples/sec, but the data were processed at the rate of 100 samples/sec. Figures 4, 5, 6, and 7 show, respectively, the time histories of acceleration, velocity, displacement, and acceleration amplitude spectra of the 5 nearest stations to the epicenter. Peak values of time histories of all stations are listed in Table 2. Table 2 also includes estimated local magnitudes, ML, for each site using the method of Kanamori and Jennings (1978). The average local magnitude, ML, of this earthquake is 6.7 ± 0.3.

The epicentral coordinates of the event given by teleseismic, regional, and strong motion data are all within several kilometers of the Bam site (Figure 2, Table 1). The location given by the strong motion data was obtained using S-P times of the four nearest stations to the earthquake. An S-P of $\sim$0.9 seconds at Bam site clearly shows that this earthquake occurred very close to the city of Bam at a distance of about 4.5 km and at a shallow depth of not more than about 5 km. This is supported by the relatively small area of damage from an earthquake of this size and also by the highly concentrated damages to Bam and its immediate vicinity. In addition, the epicenter seems to coincide with the trace of the hidden strike-slip fault inferred by Nakamura et al. (2004) from their aftershock studies. It is therefore believed that the location given by the strong motion data is more plausible than those reported by other agencies.

As shown in Figure 3, the strong motion stations are not uniformly distributed in the area. They are mostly located at the west side of the earthquake epicenter. Of all 23 triggered stations, only one site was located east of the event. In the west, 18 stations in the north and 4 stations in the south of the epicenter registered the earthquake.

The most distinctive feature of time histories at Bam site is the relatively long period pulse-shape wave forms registered shortly after the onset of P wave arrival (Figures 4, 5, 6, and 8). Propagation of a rupture toward a site at a velocity that is almost as large as the shear velocity causes most of the seismic energy from the rupture to arrive in a single large pulse of motion that occurs at the beginning of the record (Somerville et al. 1997). This pulse of motion represents the cumulative effect of almost all of the seismic radiation from the fault. In addition, the radiation pattern of shear dislocation on the fault causes this large pulse of motion to be oriented in the direction perpendicular to the fault for strike-slip faulting (Aki and Richards 1980). Forward rupture directivity effects occur when two conditions are met: the rupture front propagates toward the site, and the direction of slip on the fault is aligned with the site. In the case of strike-slip faulting, the conditions for generating forward rupture directivity are met where the fault slip direction is oriented horizontally along strike either unilaterally or bilaterally (Somerville

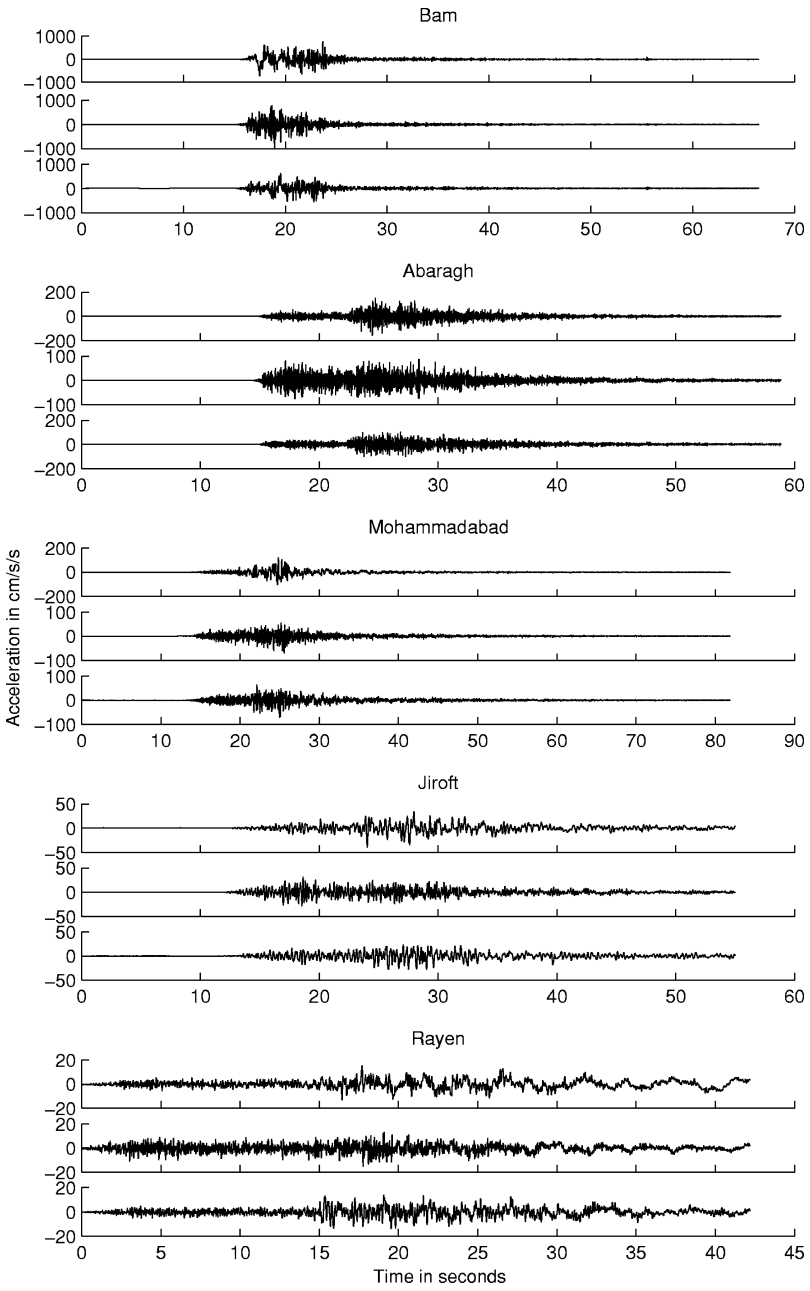

Figure 4. Digital portions of the accelerograms from the four closest stations to the center of the Bam earthquake. Station locations and component orientations are given in Table 2.

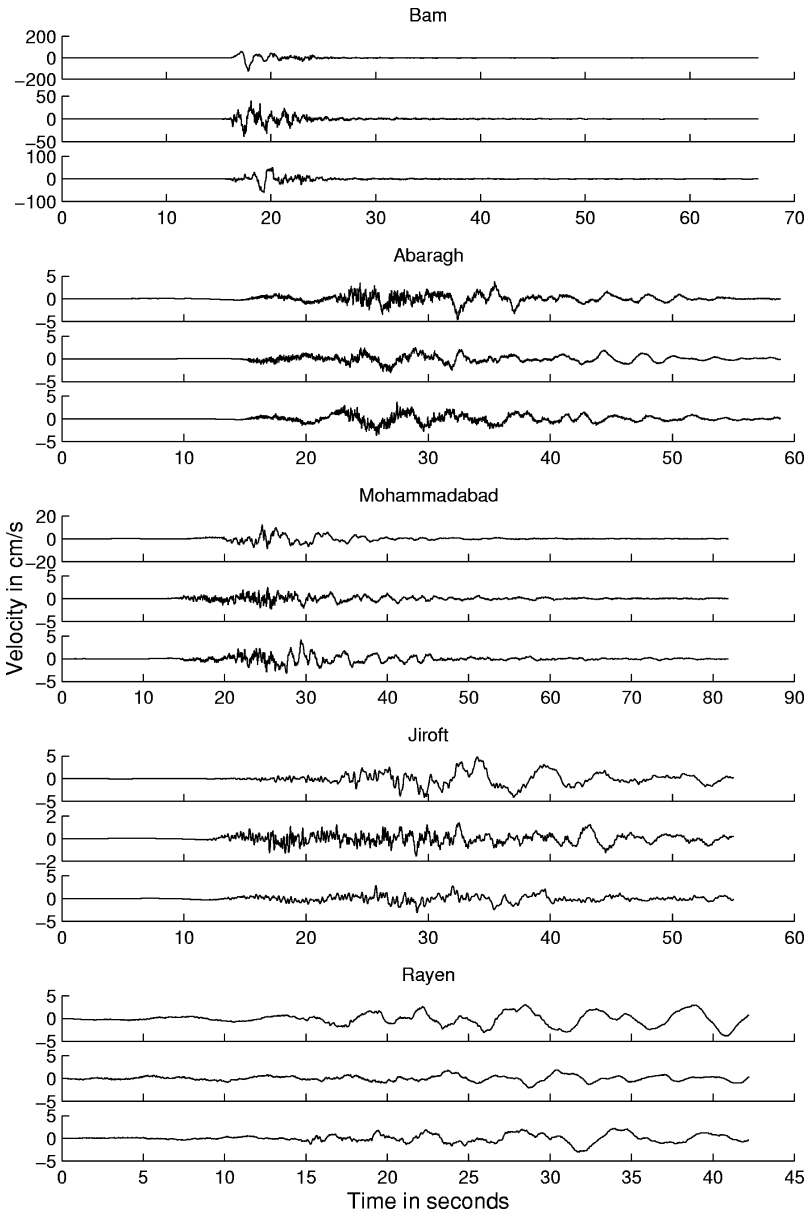

Figure 5. Velocities of ground motions, as inferred from the accelerograms from the four closest stations to the center of the Bam earthquake.

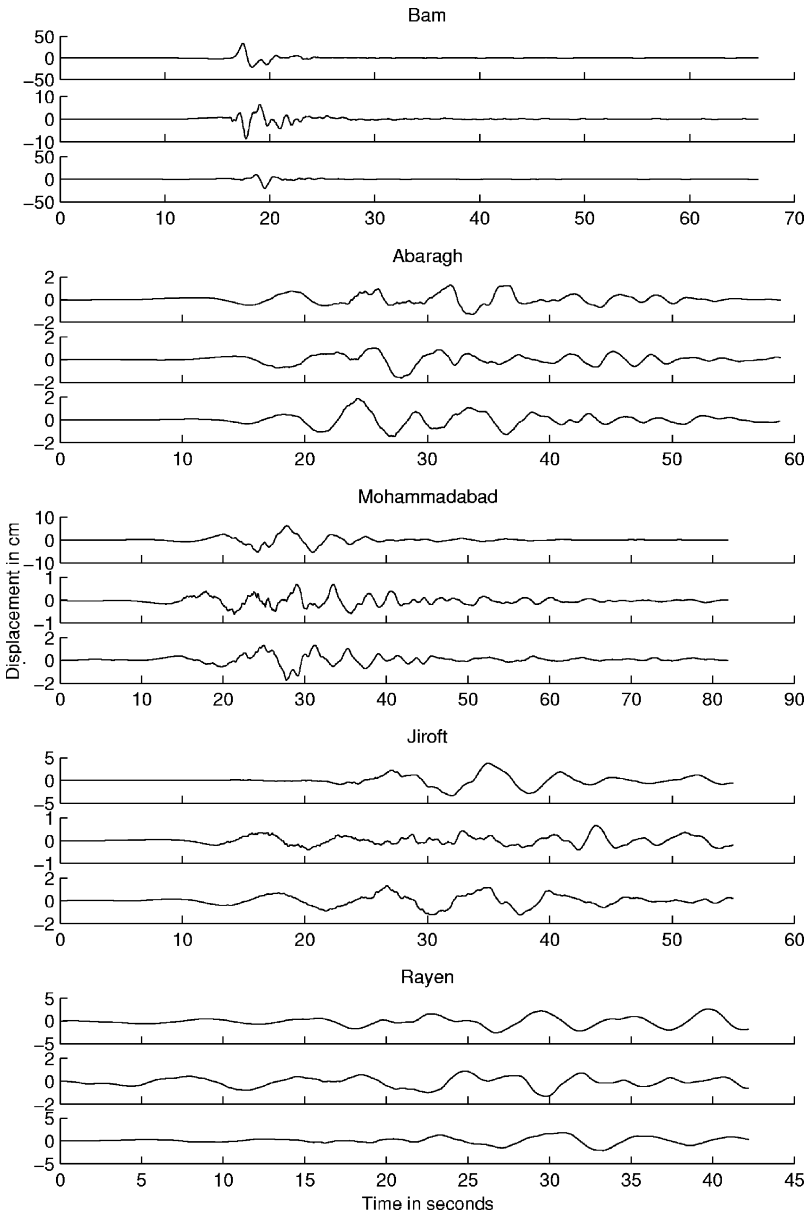

Figure 6. Displacements of ground motions as inferred from the accelerograms for the four closest stations to the center of the Bam earthquake.

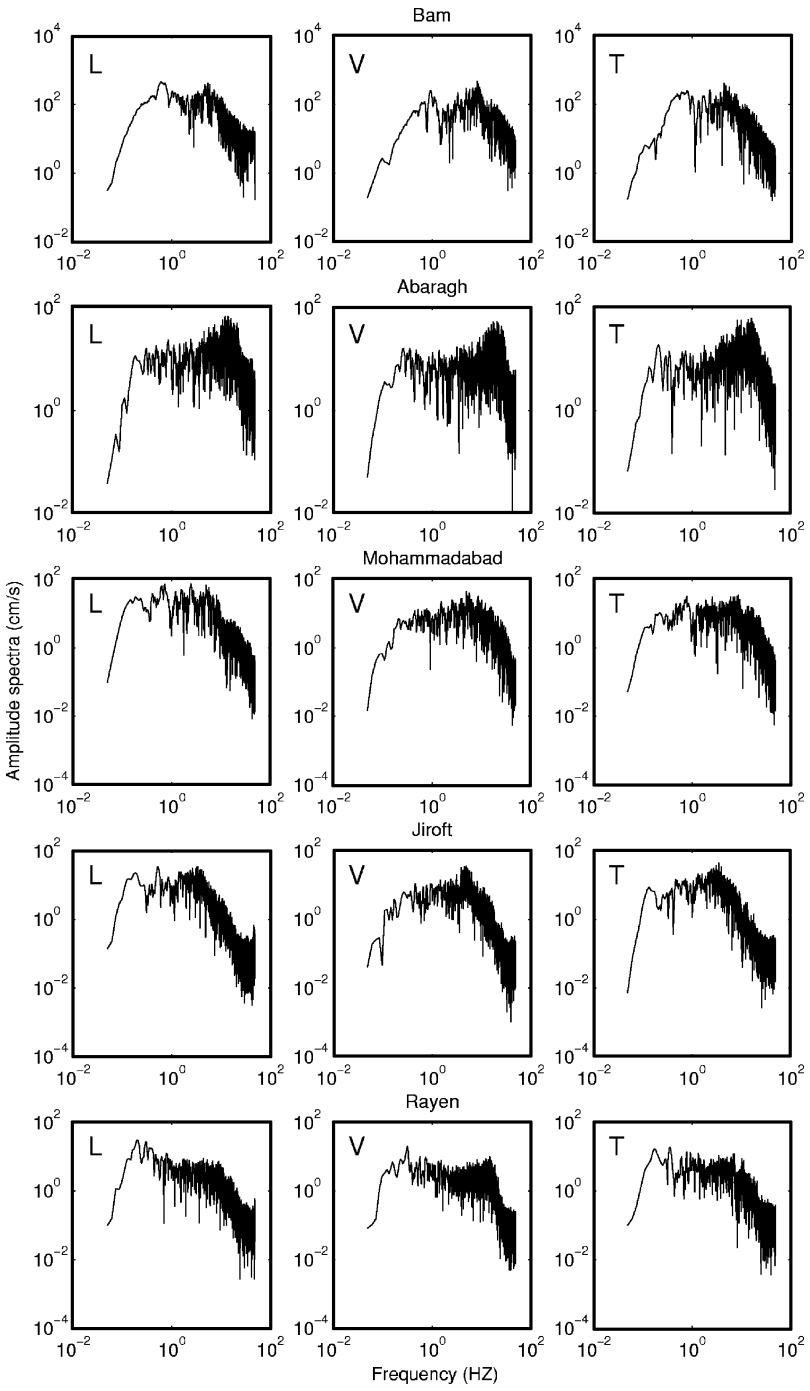

Figure 7. Fourier amplitude spectra corresponding to the accelerograms in Figure 4.

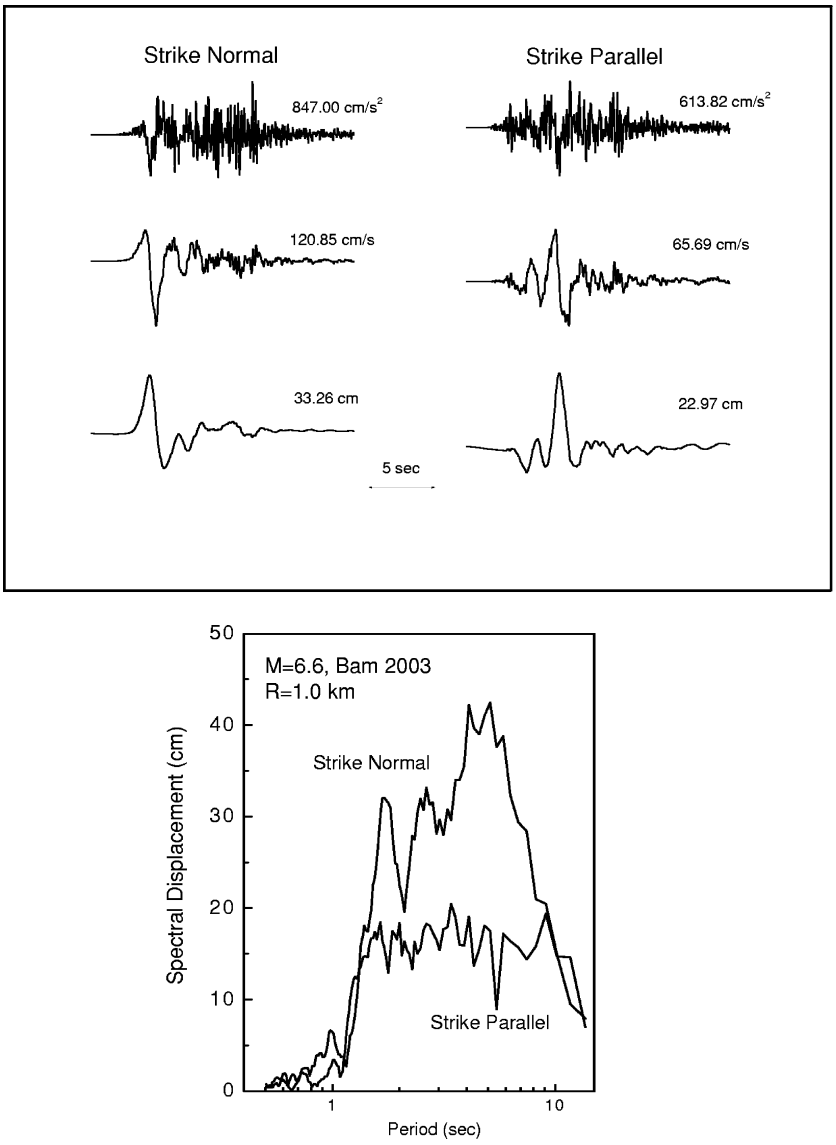

Figure 8. Top: acceleration, velocity, and displacement time histories of the strike-normal and strike-parallel components of horizontal motion recorded at Bam during the 2003 Bam earthquake. Bottom: strike-normal and strike-parallel displacement response spectra of the Bam record.

and Graves 1993; Somerville et al. 1997). In the case of the Bam earthquake, it is believed that the rupture was nucleated in the blind fault about 5 kilometers south of the city of Bam and propagated northward, passing the Bam site where it was recorded as long period pulse-shape waveforms at this station.

The top part of Figure 8 shows the acceleration, velocity, and displacement time histories of the strike-normal and strike-parallel components at Bam. There is a large difference between the strike-normal and strike-parallel motions at long periods (velocity and displacement), but this difference vanishes at short periods (acceleration). The displacement response spectrum of the strike-normal component noticeably exceeds that of the strike-parallel component for periods larger than about 1 second, as seen at the bottom of Figure 8. Somerville et al. (1997) reported similar observations on the corresponding time histories and displacement spectra recorded at Lucerne during the 1992 Landers, California, earthquake.

Figure 9 depicts particle motions of acceleration, velocity, and displacement of the Bam record on three orthogonal planes. The motions are combined using only four seconds of the beginning portion of the record to include the time duration until the rupture passes near the station. The effects of directivity are clearly shown by the appreciably larger amplitude in strike-normal direction compared with those in the other two directions at low frequencies (velocity and displacement). The vertical and parallel motions are comparable at low frequencies. At high frequencies (acceleration), while the amplitudes of vertical and strike-normal motions are comparable, the vertical motions are noticeably larger than those in parallel direction.

There are also other indications worth mentioning that may be in support, in a qualitative sense, of northward rupture propagation of faulting during this earthquake. Briefly: Over 80% of the triggered stations with a distance range of 5 to 290 km are located in the northern section of the epicenter, whereas, in the southern part, only four stations with a maximum epicentral distance of ~170 km registered the event (Figure 3, Table 2). At Bam station, about 5 km north of the epicenter (less than 1 km from the rupture), the recorded PGA and PGV in both horizontal and vertical components were exceptionally large for an event of this size, Abaragh and Mohammadabad stations, located at the north and south of the event, have about the same epicentral distances and the site geology of both stations are also similar as reported by Mirzaei and Farzanegan (1998). As depicted in Figures 7 and 10, the spectra from Abaragh show broad, pronounced amplitudes at high frequencies on all three components at this site. Comparison between acceleration spectra of these two stations show that at high frequencies, the spectral amplitudes at Abaragh are more than one order of magnitude larger than those at Mohammadabad station.

RUPTURE VELOCITY

Figure 11 shows the onsets of P waves and S waves and the time of the rupture front arriving at the Bam station. Based on S-wave and P-wave velocities of 3.3 km/sec and 5.7 km/sec, and employing the S-P time interval of 0.90 sec and the time interval of 0.75 sec. between the arrival of the rupture front and the S wave, we estimated a northward rupture velocity of about 2.5±0.2 km/sec for this earthquake.

PEAK VALUES, ATTENUATIONS

Figure 12 plots the horizontal and vertical peak ground accelerations, recorded at 23 stations, against the closest distances, ranging from 1 to 288 km from the blind fault that

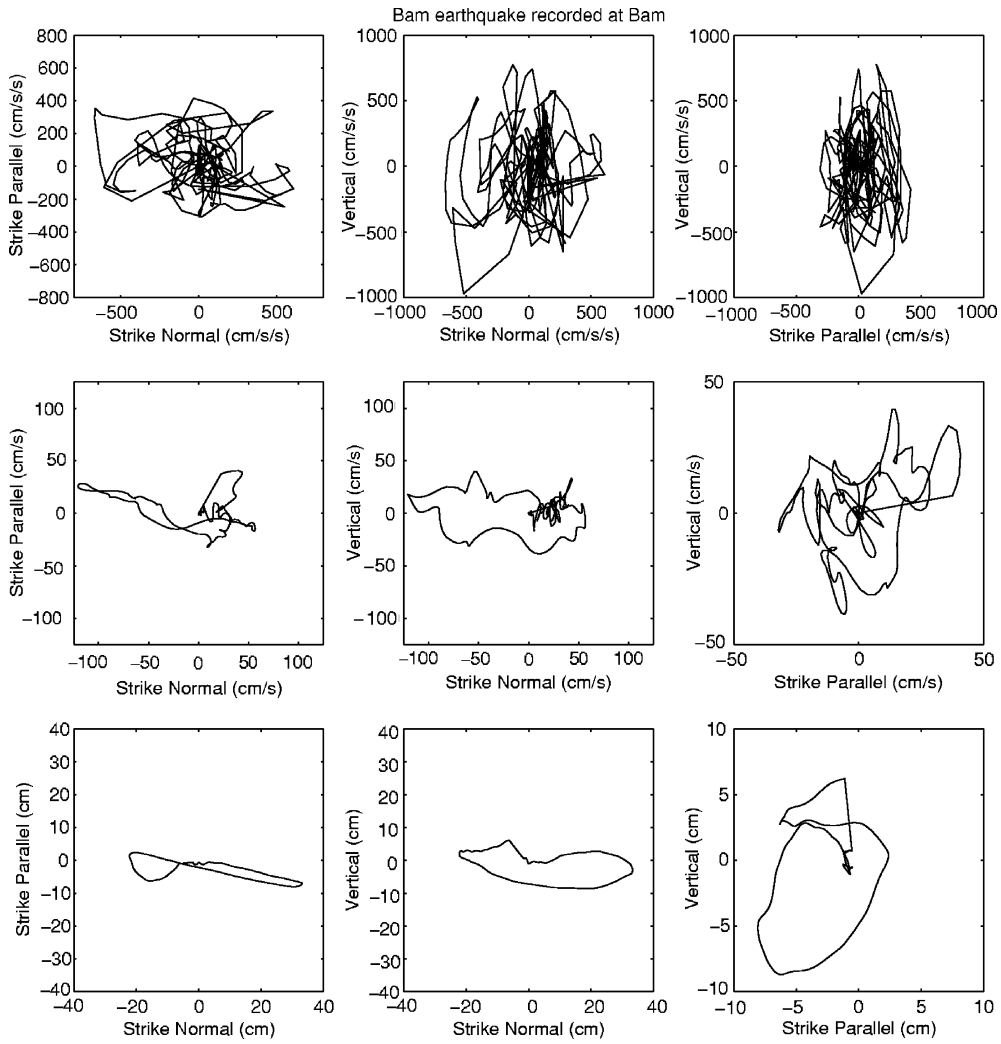

Figure 9. Particle motions of acceleration, velocity, and displacement of the Bam record on three orthogonal planes. The effects of directivity are shown by the pronounced amplitude in the strike-normal direction at low frequencies (velocity and displacement).

has been inferred by other investigators (e.g., Nakamura et al. 2004). In this distance range, about 46 stations were operational at the time of the earthquake. Reygan station, about 80 km from the source, was not operational because of battery malfunctioning. Fahraj station, located about 50 km to the east of the source, was the nearest site that did not register the earthquake (personal communication with staff at BHRC).

Figure 12 shows the plots (solid lines) of the horizontal (average of two components) and vertical ground accelerations against distance recorded at 23 stations. These peaks

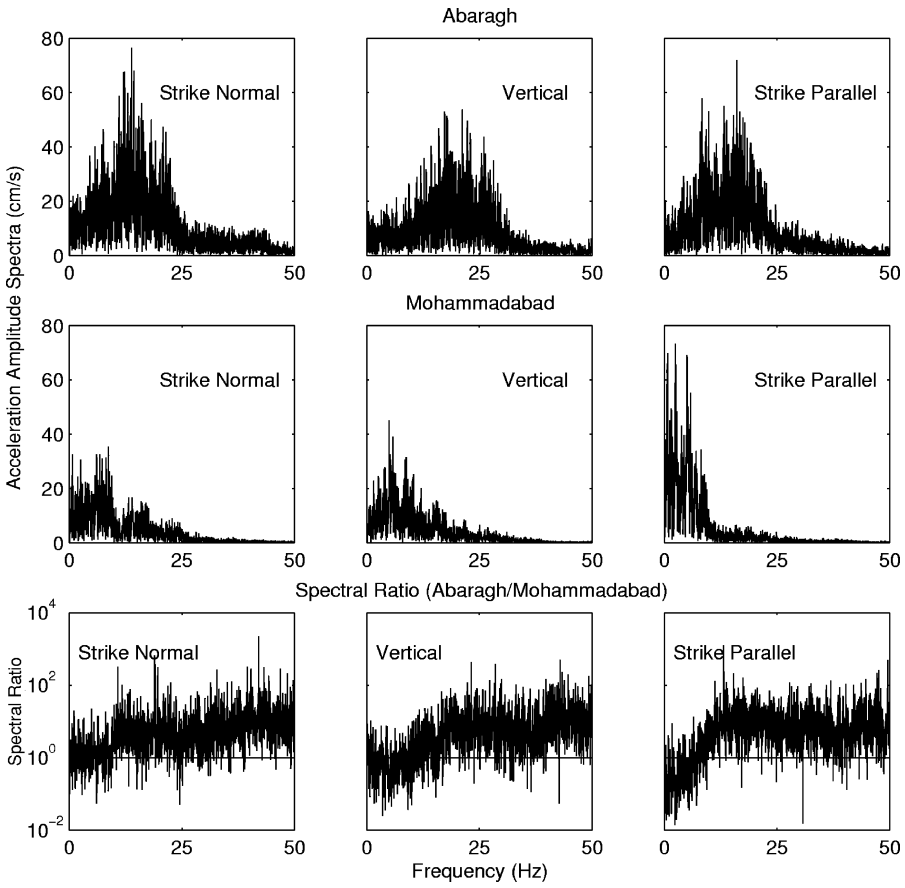

Figure 10. Acceleration spectra of Abaragh and Mohammadabad stations and their corresponding spectral ratios. Note the broad, pronounced amplitude at high frequencies on all components of the Abaragh station.

were compared with 50% peak ground acceleration prediction curves introduced by Shoja-Taheri (2002) for the east-central region of Iran for M_w=6.5 (dashed lines in Figures 12c and 12d). They were also compared with the new prediction curves for the region, modified in this study, by including the Bam records (dashed lines in Figures 12a and 12b).

In fitting the curves both to the regional and the Bam data, a form similar to that of Joyner and Boore (1981) has been chosen, but with a fixed magnitude for the Bam data.

$$\text{Log}\, P = A + BM_w - \text{Log}\, R - CR \tag{1}$$

$$R = (d^2 + h^2)^{1/2}$$

In Equation (1), P is the peak value of the ground motion parameter of interest, d is

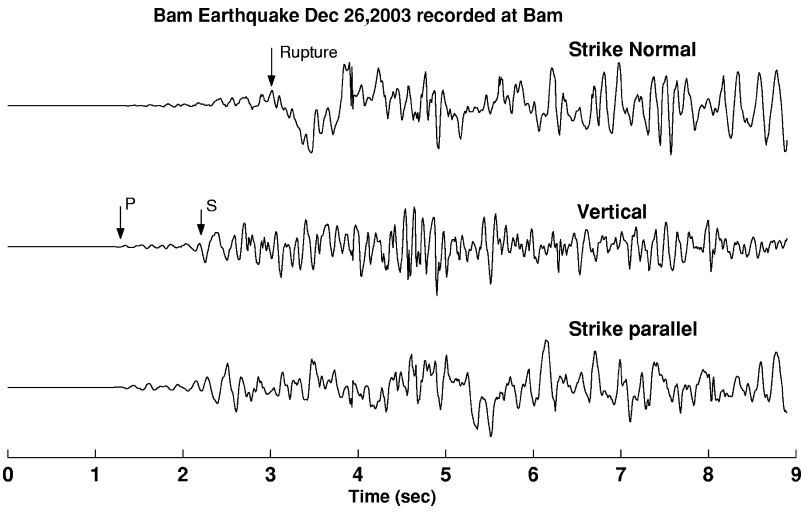

Figure 11. Digital portions of acceleration time histories of the Bam record. Rupture velocity of 2.5±0.2 km/sec inferred from S-P, the arrival times of S-waves, and the rupture front passing the Bam station.

the nearest distance to the fault surface, h compensates for energy release occurring away from the nearest point on the fault surface, and C represents the inelastic decay parameter. The numerical values of $A+B$, M_w, C, and h for the Bam data are shown in Figure 12 for peak horizontal acceleration, PHA, and peak vertical acceleration, PVA. The value of $h=5.0$ km was arbitrarily selected for the Bam data to be consistent with the shallow depth of about 5 km inferred. To compare the Bam data with the attenuation relations previously found for the region (Shoja-Taheri 2002), the coefficient of Log R was constrained to be 1.0 for the Bam data, assuming that for close distances to a point source, body waves have the major contribution in characterizing peak values.

As seen in Figure 12, the large values of both horizontal and vertical peaks recorded at Bam site caused significant deviations, at the near source, between the attenuation curves of the Bam earthquake and those predicted for the region. The PHA discrepancies between the curves are diminished at large distances. However, the difference between the PVA curves remains noticeable at all distances and this is due to the very large value of PVA (about 970 cm/sec^2) recorded at Bam station.

Incorporating the Bam data to modify the regional attenuation curves also introduced pronounced near field differences between the existing and the modified curves derived for the region. These differences are obviously produced by the effects of the forward directivity observed at Bam site. For seismic design studies in an area such as Bam city, it is, therefore, an important decision making to what extent the effects of directivity should be taken into account.

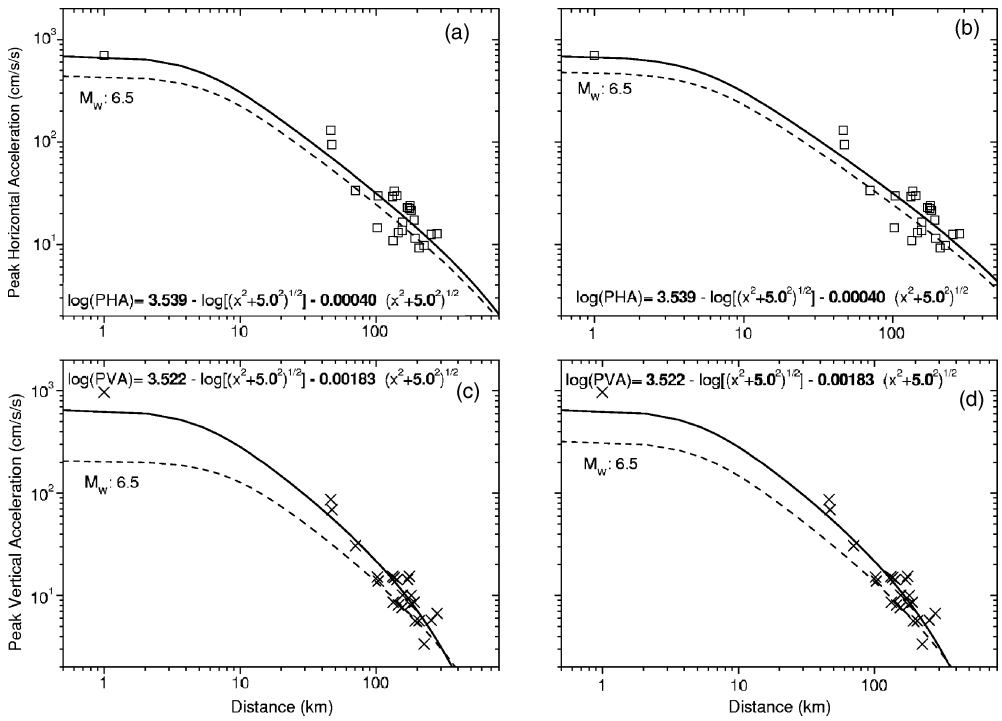

Figure 12. Distance dependence of peak horizontal (average of two components) and peak vertical accelerations for Bam earthquake (solid lines). Dashed lines correspond to the attenuation curves of the east-central region of Iran. The regional curves in (a) and (c) have been reported by Shoja-Taheri (2001), whereas the curves in (b) and (d) were developed in this study by including the Bam data (see also Table 3).

Employing the numerical values of the regional PHA curves at large distance (e.g., 100 km) as a reference, a magnitude of 6.8±0.2 is estimated from the Bam PHA prediction relations shown in Figure 12.

SPECTRA

Fourier spectra corresponding to each accelerogaram were calculated (spectra of the five nearest stations from Bam source are shown in Figure 7). Except for local variations, they generally show a decrease in amplitude of shaking with distance. The spectra from Abaragh show a broad, pronounced high amplification on horizontal and vertical components centered at about 15 Hz (Figures 7 and 10).

We have characterized these spectra following the method of Anderson and Hough (1984), in which the trend of the spectra at high frequencies is described by the function $a(f)=A_0 \times e^{-\pi \kappa f}$ where κ (kappa) is the spectral decay parameter and A_0 gives the overall level. Figure 13 plots the values of A_0 and κ determined from the whole record spectra over the frequency band of 2 to 15 Hz as a function of distance (Table 2). As in Shoja-

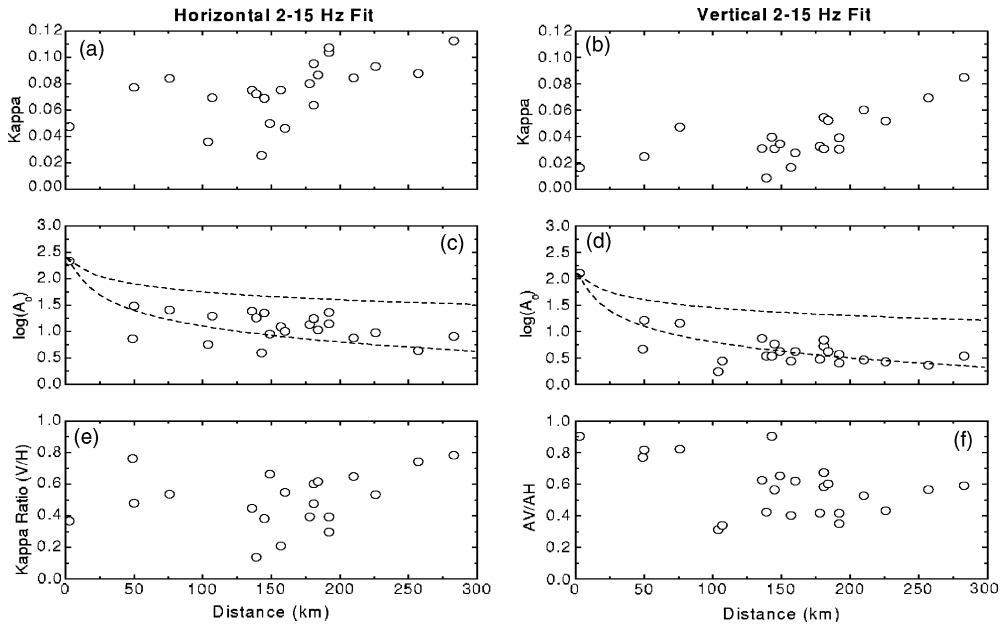

Figure 13. Decay parameter, κ, and overall level, A_0, from the Bam spectra as a function of distance.

Taheri and Anderson (1988), the present study found that the spectra are generally fit satisfactorily by the exponential decay model. The most severe exception was the horizontal and vertical components at Abaragh, where the κ's become negative because of the strong amplification at high frequencies at this site. κ 's for vertical components of Rayan and Golbaf stations were also negative. These values are about 0.04 sec at the nearest station and increase gradually with distance at a rate comparable to that observed from the 1978 Tabas, Iran earthquake (Shoja-Taheri and Anderson 1988). This increase in κ with distance can only be an effect of attenuation. Comparing the rate to that found in California (Anderson and Hough 1984; Anderson 1986) confirms that the attenuation in the east-central region of Iran appears to be about the same as in California. We find that the κ from vertical components of these records are considerably smaller than the κ's for the horizontal components. Similar observation was made from the records of the 1978 Tabas earthquake. The plot of vertical to horizontal ratio of κ in Figure 13 shows that the ratio has also a gradual increase with distance.

Figure 13 also shows the values of A_0 plotted as a function of distance for the horizontal and vertical spectra. These values are compared with attenuation curves proportional to $r^{-0.5}$ and $r^{-1.0}$. Consistent with these regression results, the falloff is between these two values. The horizontal and vertical spectra falloff as $r^{-0.7}$ and $r^{-0.9}$, respectively.

SEISMIC ENERGY

It is important to calculate the radiated energy. From the Bam records we can provide a near-field test of the relationship proposed by Gutenberg and Richter (1954) based on the teleseismic data. In addition, the energy density represented by an individual seismogram has engineering applications for nonlinear analysis. One method of estimating energy is to directly integrate the observed waveforms at one (or more) station and to infer energy based on the energy flux expected at the station, as determined by the geometry.

Following Shoja-Taheri and Anderson (1988), this study began by defining the integrals:

$$I_t(t) = \int_{\infty}^{\infty} v^2(t)dt \tag{2}$$

$$I_f(f) = \int_{0}^{\infty} \tilde{v}^2(f)df \tag{3}$$

where $\tilde{v}(f)$ is the Fourier transform of the velocity, $v(t)$. Note that $I_t(\infty)=I_f(\infty)$. As was observed by Vassiliou and Kanamori (1982) and by Shoja-Taheri and Anderson (1988), by far most of the radiated energy is in waves with frequencies less than 1 to 2 Hz. This result was confirmed with other stations. For a station near a finite fault, the relationship between integrated velocity and total radiation energy includes a geometrical term, which depends on fault geometry, distance, radiation pattern, and focusing due to rupture propagation. Consider a surface, Σ, with area S_a that surrounds the fault. Then, provided all of the energy is flowing outward from the fault, the radiated energy could be obtained from a sufficiently dense sampling of $I_t(\infty)$ over Σ. With less data, one can assume that a single station is representative of every point on Σ. The energy thus estimated from a single observation point may be approximately written as:

$$E = 1/4\rho\beta S_a I_t(\infty) \tag{4}$$

In Equation (4), it was assumed that all the waves cross the surface with velocity β. The density of the material is ρ. The quantity $\rho\beta I_t(\infty)$ is the energy flux (from Bullen and Bolt 1985). The factor of $1/4$ comes from an assumption that observed velocities have been doubled by the surface of the earth. According to Bullen (1963) and Bolt (1986), errors introduced by this doubling assumption is generally less than 20%.

For large distances, R, compared to the fault dimension, the area S_a is the surface area of a sphere that surrounds the fault (Båth 1966):

$$S_a = 4\pi R^2 \tag{5}$$

Trifunac (1972) and Anderson et al. (1986) approached the geometrical problem for strong motion stations directly above the fault by assuming the stations sampled the wave field from a uniformly radiating rupture of area A. Under this approach:

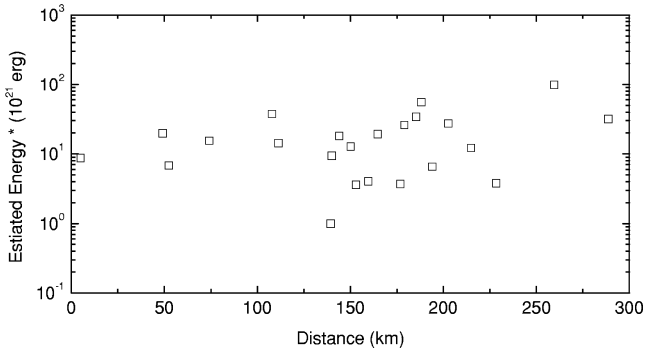

Figure 14. Energy estimates for the Bam earthquake shown as a function of distance of the stations to the fault. Results were obtained using ellipsoidal normalization.

$$S_a = 2A \tag{6}$$

For the Bam geometry, S_a was evaluated employing the scheme introduced by Shoja-Taheri and Anderson (1988), which they refer to as "ellipsoidal normalization." In this approach, S_a is asymptotic to a close bound for elliptical approximation of the fault area for a short distance to the fault and asymptotic to a sphere for large distance, R, compared to the fault dimension. Therefore, it provides a smooth transition between the two cases given by Equations (5 and 6). S_a was found numerically, as were the energy estimates for all the stations recording the earthquake. In Figure 14, the energy estimates are shown as a function of distance of the station to the fault. The geometric average of all 23 stations is 1.2×1022 ergs, which corresponds to M_s=6.8. The geometric mean was used rather than the arithmetic mean because the arithmetic mean is not dominated by one or two outliers, and because residuals on regressions which are also affected by site effects show a lognormal distribution.).

This magnitude estimate agrees with that estimated by the peak values of the synthetic Wood-Anderson accelerograms and also with the magnitude inferred from the proposed attenuation relation for this earthquake (Table 2, Figure 12).

These energy estimates can be compared with estimates arrived at by other procedures. A static estimate for the energy from moment (Vassiliou and Kanamori 1982) is 5.0×1021 ergs, a factor of 2 less than the present estimates from the seismograms. This energy estimate (1.2×1022 ergs) agrees with the Gutenberg and Richter (1954) energy formula with M_s=6.8, which gives $E = 1.0 \times 10^{22}$ ergs.

This energy estimate neglected the difference between geometrical spreading in an infinite medium and in the earth, where energy is trapped near the surface. In Figure 14, this effect would show an increase in the estimated energy with greater distance as the result of increasing contribution of surface waves.

There are several indications that site effects may be important at some stations. However, since no detailed profiles of the structure below the sites are available, it was not thought prudent to consider any effects due to site geology in this analysis.

Theoretical relations involving seismic source parameters are employed here in an attempt to estimate the various source parameters of the Bam earthquake.

The seismic moment $M_0(S)$ is determined from the S-wave spectrum through the relation

$$M_0(S) = \frac{\Omega_0(S)}{\Re_{\theta\phi}(S)} 4\pi\rho R\beta^3 \quad \text{(Keilis-Borok 1960)} \tag{7}$$

where:

$M_0(S)$ = Seismic moment determined by the S-wave spectrum
$\Omega_0(S)$ = Long-period spectral level of the S wave
$\Re_{\theta\phi}(S)$ = Radiation pattern for the S wave
ρ = Density = 2.7 gm/cm^3
R = Accounts for spreading in a layered media
β = Shear wave velocity = 3.3 km/sec

The source dimension is given by:

$$r(S) = \frac{2.34\beta}{2\pi f_0(S)} \text{corrected from Brune (1970) by Brune (1971)} \tag{8}$$

where:

$r(S)$ = Radius of a circular source area determined by the S-wave spectrum
$f_0(S)$ = Corner (peak) frequency of the S-wave spectrum.

The stress drop is given by:

$$\Delta\sigma = \frac{7}{16}\frac{M_0}{r^3} \text{corrected from Brune (1970) by Brune (1971)} \tag{9}$$

Figure 15 plots the accelerograms and the corresponding S-wave source displacement spectra of the horizontal components for the four stations nearest the Bam epicenter. The arrows show the S-wave time windows, which were employed for spectral calculations. The acceleration records of Bam station were not included here because the train of S-waves in this site is dominantly overlapped by the recorded rupture front passing near this site. The displacement spectra of the S-waves were corrected for a frequency-dependent quality factor, $Q=350f$, and for the decay parameter, κ, evaluated for each record. Equations 7–9 were then used to estimate the seismic moment, $M_0(S)$, source radius, r, and stress drop, $\Delta\sigma$, for this earthquake. Table 3 lists the results. The average of $M_0 = 8.3 \times 0^{25}$(dyne-cm) gives a moment magnitude of $M_w = 6.6$ for this earthquake. The estimates of source radius and the stress drop are ~7.5 km and ~90 bars, respectively. These estimates agree well with the estimates obtained by analy-

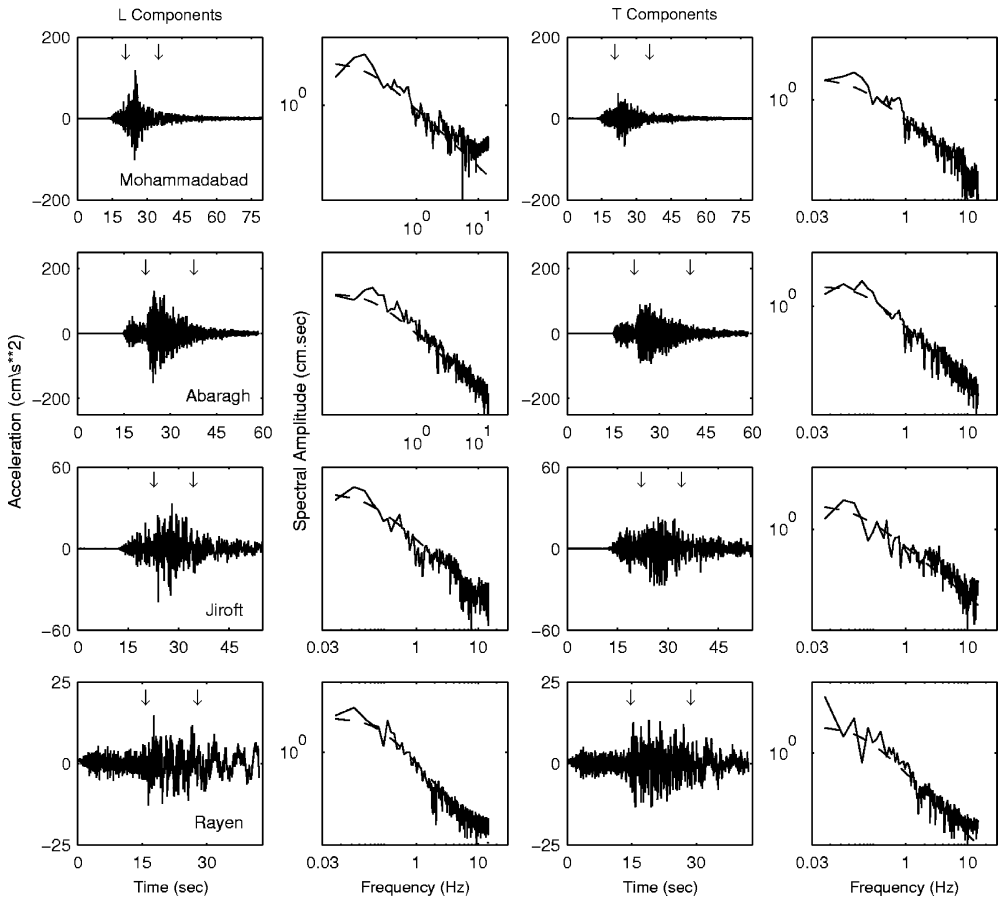

Figure 15. Accelerations and the corresponding S-wave displacement spectra of horizontal components for the four stations closest to the Bam epicenter. The arrows show the S-wave time windows used for spectral calculations.

sis of the regional broadband seismograms provided by the Khorasan Seismic Network of Ferdowsi University of Mashad (Table 3). The estimates are also in good agreement with those obtained from telemetric data (Table 1).

CONCLUSIONS

The strong motion records of the 2003 Bam earthquake were interpreted to investigate the complexity of the source of this earthquake in some detail, construct attenuation curves for values of horizontal and vertical accelerations, and estimate some of the source parameters such as seismic energy release, seismic moment, and stress drops. The results are summarized as follows.

Table 3. Bam earthquake source parameters obtained from strong motion data

Station	Epicentral distance	$M_0 \times 10^{25}$ dyne-cm	M_w	f_0(Hz)	r source radius (km)	Stress drop bar
Mohammadabad	49.1	09.10	6.6	0.15	8.2	73
Abaragh	52.4	03.91	6.4	0.19	6.5	62
Jiroft	74.1	12.45	6.7	0.15	8.2	99
Rayan	107.9	10.57	6.6	0.18	6.8	147
Geometrical average		08.27	6.6	0.17	7.4	90

1. The compact and pulse-shape arrivals of strong signals on the Bam records strongly suggest that the rupture was initiated in the reported blind fault near the south of the city of Bam and propagated toward the Bam site. The inferred epicenter from the strong motion records is about 5 km south of Bam and several kilometers north of the reported epicenters. Based on the relative arrival times of the rupture front and P and S waves at this station, the velocity of rupture was estimated as 2.5 ± 0.2 km/sec.
2. The peak values of both horizontal and vertical accelerations of the Bam earthquake were employed to infer attenuation curves for this earthquake. Comparison of these peak values with the regional prediction curves shows that the effects of forward directivity at the Bam site caused significant deviations between the curves at near source distance. The comparison between the curves at large distance gives a magnitude of 6.8 ± 0.2 for this earthquake.
3. Total radiated energy was estimated for "ellipsoidal normalization" procedures, for which the geometric average of energy of 23 stations is 1.2×10^{22} ergs. This energy estimate agrees with the Gutenberg and Richter formula with $M_s = 6.8$.
4. Theoretical relations involving source parameters were used to estimate some of the source parameters of the Bam earthquake. Employing S-wave displacement spectra of horizontal components for the four stations near the Bam epicenter, the seismic moment was estimated as $M_0 = 8.3 \times 0^{25}$ (dyne-cm), which gives a moment magnitude of $M_w = 6.6$ for this earthquake. The estimates of source radius and stress drop are about 7.5 km and 90 bars, respectively. These estimates are consistent with estimates developed by analysis of the regional broad-band seismograms. They are also in good agreement with those obtained from telemetric data.

ACKNOWLEDGMENTS[1]

The authors would like to thank Dr. G. Haidarinejad of Building and Housing Research Center (BHRC), Ministry of Housing and Urban Development, who gave permission for the use of the strong motion data of the Bam earthquake in this study. The assistance of all the staff at Iran Strong Motion Network is greatly appreciated.

REFERENCES

Adeli, H., 1982. The Sirch (Kerman, Iran) earthquake of 28 July 1981—A field investigation, *Bull. Seismol. Soc. Am.* **72**, 841–861.

Aki, K., and Richards, P. G., 1980. *Quantitative Seismology: Theory and Methods*, W. H. Freeman, San Francisco, Vol. 1, 558 pp.

Ambraseys, N. N., and Melville, C. P., 1982. *A History of Persian Earthquakes*, Cambridge University Press, Cambridge.

Anderson, J. G., 1986. Implication of attenuation for studies of the earthquake source, *Earthquake Source Mechanics*, edited by S. Das, J. Boatwright, and C. H. Scholz, Geophysics Monograph 37, Maurice Ewing Series 6, American Geophysical Union, Washington, D.C., pp. 311–318.

Anderson, J. G., and Hough, S. E., 1984. A model for the shape of the Fourier amplitude of spectrum of acceleration at high frequencies, *Bull. Seismol. Soc. Am.* **73**, 1969–1994.

Anderson, J. G., Bodin, P., Brune, J., Prince, J., Singh, S. K., Quaas, R., and Onate, M., 1986. Strong ground motion from the Michoacan, Mexico earthquake, *Science* **233**, 1043–1049.

Båth, M., 1966. Earthquake energy and magnitude, *Physics and Chemistry of the Earth*. Edited by L. H. Ahrens, F. Press, S. K. Runcom, and H. C. Urey, Pergamon Press, Oxford, England, Vol. 7, pp. 117–165.

Berberian, M., Jackson, J., Ghorashi, M., and Kajar, M. H., 1984. Field and teleseismic observations of the 1981 Golbaf-Sirch earthquakes in SE Iran, *Geophys. J. R. Astron. Soc.* **77**, 809–838.

Bolt, B. A., 1986. Seismic energy release over a broad frequency band, *PAGEOPH* **124**, 919–930.

Brune, J., 1970. Tectonic stress and the spectra of seismic shear waves from earthquakes, *J. Geophys. Res.* **75**, 4997–5009.

Brune, J., 1971. Correction, *J. Geophys. Res.* **76**, 5002.

Bullen, K. E., and Bolt, B. A., 1985. *An Introduction to the Theory of Seismology*, 4th ed., Cambridge University Press, Cambridge, England, 499 pp.

Gutenberg, B., and Richter, C. F., 1954. *Seismicity of the Earth and Associated Phenomena*, Princeton University Press, Princeton, NJ.

[1] Publication of this special issue on the Bam, Iran, earthquake was supported by the Learning from Earthquakes Program of the Earthquake Engineering Research Institute, with funding from the National Science Foundation under grant CMS-0131895. Any opinions, findings, conclusions, or recommendations expressed herein are the authors' and do not necessarily reflect the views of the National Science Foundation, the Earthquake Engineering Research Institute, or the authors' organizations.

Iran Strong Motion Network (ISMN), Building and Housing Research Center (BHRC), Ministry of Housing & Urban development; http://www.bhrc.gov.ir.

Joyner, W. B., and Boore, D. M., 1981. Peak horizontal acceleration and velocity from strong-motion records including records from the 1979 Imperial Valley, California, earthquake, *Bull. Seismol. Soc. Am.* **71**, 2011–2038.

Kanamori, H., and Jennings, P. C., 1978. Determination of local magnitude, M_L, from strong-motion accelerograms, *Bull. Seismol. Soc. Am.* **68**, 471–485.

Keilis-Borok, V. I., 1960. Investigation of the mechanism of earthquake, *Sov. Res. Geophys.* (English transl.) **4**, 29.

Mirzaeialavijeh, H., and Farzanegan, E., 1998. Specifications of the Iranian Accelerograph Network Stations, Building and Housing Research Center, Publication No. 280.

Nakamura, T., Suzuki, S., Matsushima, T., Ito, Y., Keivan-Hosseini, S., Gandomi, A. J., Sadeghi, H., Maleki, M., and Fatemi-Aghda, S. M., 2005. Source fault structure of the 2003 Bam earthquake, southeastern Iran, inferred from the aftershock distribution and its relation to the heavily damaged area: Existence of the Arg-e-Bam fault proposed, 2004. Submitted for publication.

Shoja-Taheri, J., 2002. Attenuation relations for peak and response spectra of horizontal acceleration from strong-motion records for the main seismic zones of the Iranian Plateau, *Seismol. Res. Lett.* **73**, 242 (SSA Meet. Suppl.), abstract.

Shoja-Taheri, J., and Anderson, J. G., 1988. The 1978 Tabas, Iran, earthquake: An interpretation of the strong motion records, *Bull. Seismol. Soc. Am.* **78**, 142–171.

Somerville, P. G., and Graves, R. W., 1993. Conditions that give rise to unusually large long period ground motion, *Struct. Des. Tall Build.* **2**, 211–232.

Somerville, P. G., Smith, N. F., Graves, R. W., and Abrahamson, N. A., 1997. Modification of empirical strong ground motion attenuation relations to include the amplitude and duration effects of rupture directivity, *Seismol. Res. Lett.* **68**, 199–222.

Talebian, M., Fielding, E. J., Funning, G. J., Ghorashi, M., Jackson, J., Nazari, H., Parson, B., Priestley, K., Rosen, P. A., Walker, R., and Wright, T. J., 2004. The Bam (Iran) earthquake: Rupture of a blind strike-slip fault, *Geophys. Res. Lett.* **31**, L11611, doi:.10.1029/2004G1020058.

Trifunac, M. D., 1972. Stress estimates for the San Fernando, California earthquake of February 9, 1971: Main event and thirteen aftershocks, *Bull. Seismol. Soc. Am.* **62**, 724–750.

Vassiliou, M. S., and Kanamori, H., 1982. The energy release in earthquakes, *Bull. Seismol. Soc. Am.* **72**, 371–384.

Yagi, Y., 2004. Preliminary results of rupture process for 2003 December 26 southeastern Iran earthquake: Source process of recent large earthquakes, international institute of Seismology and earthquake engineering; available at http://iisee.kenken.go.jp/staff/yagi/eq/Iran20031226/IRAN20031226.htm

(Received 18 October 2004; accepted 29 April 2005)